Static and dynamic impulses generated by two-phase detonations

Shmuel Eidelman[a] and Martin Sichel

Department of Aerospace Engineering, The University of Michigan, Ann Arbor, Michigan 48109
(Received 1 December 1980; accepted 14 October 1981)

The influence of the mixture density and the reaction zone length on the static and dynamic impulse of the detonations through wheat dust, RDX dust, and decane droplet air mixtures was studied. A numerical solution of the detailed model of the two-phase detonation initiation and development in the medium provided the basis for the study. Mixtures with a higher average density were found to produce a significantly greater static impulse, but a reduced dynamic impulse. The reasons for this behavior were discussed.

I. INTRODUCTION

A comparison of the damage produced by charges of equal energy of explosion but with different physical, chemical, and geometrical parameters was first discussed by Brode[1,2] in an earlier publication on the numerical calculation of the explosion process. In this work he studied the influence of the geometrical size of the exploding charge on the dynamics of blast propagation, and on the shock wave overpressure as a function of distance from the charge surface. He compared the blast wave produced by a point explosion, a TNT charge, and a bursting sphere of equal energies and found that the parameters of the shock waves become equal at a relatively large distance from the source of the explosion (~20 TNT charge radii).

Fishburn[3] compared the peak overpressure and the static and dynamic impulses for a centrally initiated detonation, a high pressure sphere, an ideal point source, an implosion, and detonating and deflagrating fuel-air mixture. Sternberg and Hurwitz[4] compared the energy distribution behind shock waves produced by solid explosive charges with different physical and chemical parameters.

There appear to be no corresponding comparative experimental studies, probably because the expected difference in wave parameters is smaller than can be resolved experimentally. In the above-mentioned work, only gaseous or solid explosives were considered, and the parameters of the detonation wave were calculated using self-similar detonation solutions or numerical solutions using heat addition in the vicinity of the shock wave to reproduce the Chapman–Jouguet (C–J)-like detonation structure. At the same time, recent experimental investigations of two-phase detonation phenomena[5] show that the structure of two-phase detonations is appreciably different from that of gaseous detonations. Reaction zone lengths are comparatively long depending on the physical and chemical parameters of the mixture, and can no longer be considered as a discontinuity as in the classical C–J model. Recently, attention has focused on the detonation of different dusts in air. The projected increased need for coal as an energy source and different techniques for making coal a more "convenient and transportable" fuel in turn require improved techniques for preventing dust explosions.

Numerous grain elevator explosions have stimulated the investigation of the detonation properties of different grain dusts in air and oxygen.[6] Some detonating dusts contain their own oxidizer; and then, the detonation parameters are no longer limited by the amount of oxygen in air, and high concentrations of dust in the detonable mixture can more than double the average density of the mixture compared with a gaseous mixture with the same detonation parameters.

In the present study numerical modeling is used to determine how in two-phase detonations the higher density of the detonating mixture and the greater reaction zone length influence the dynamic and static impulse, wave overpressure, and the structure of the detonation wave, which in turn determine the extent of explosion damage.

II. THE MATHEMATICAL MODEL AND NUMERICAL SOLUTION

In order to stimulate the direct initiation and propagation of detonation waves through two-phase reactive media it is necessary to develop a mathematical model which describes the separate motion of each of the phases and the energy, momentum, and mass exchange between them.

A model capable of simulating this problem has been developed and is described in detail by Eidelman and Burcat.[7,8] The present work presents results obtained using this model. Nevertheless, a brief description and summary of the formulation is included for completeness. The conservation equations are written separately in Eulerian form for the solid fuel phase and the gaseous oxidizer. The conservation equations of the two phases are interconnected through source terms on the right-hand sides of the equations. The fuel particles are considered to behave as a continuous medium composed of noninteracting spheres whose size is equal to the average size of the particles. It is assumed that chemical reactions occur only in the gas phase, and that the burning rate of the particles is determined by the rate of evaporation. This assumption implies that the burning rate in the gas phase is much faster than the rate of particle evaporation.

[a]Current address: Department of Aeronautics, Naval Post graduate School, Monterey, California 93940.

 0031-9171/82/010038-07$1.90

The chemical physics of solid particle disintegration and burning behind a strong shock wave are unknown in detail and will probably be different from one type of particle to another. In addition to the chemical and physical parameters disintegration will also depend on the structure of the solid material of the particle. It has not been possible to find theoretical or experimental work describing solid particle disintegration and burning behind strong shock waves. Most of the numerical simulations of solid-gas detonation[9,10] use rapid evaporation models with empirical coefficients to produce realistic reaction zone lengths.

In the present work experimental reaction zone measurements[6] were used to define the coefficients in a combined evaporation and shattering model to reproduce the reaction zone lengths observed in experiments. The equations expressing the conservation of mass, momentum, and energy for the two phases are written in a uniform way as

$$\frac{\partial A}{\partial t}+\frac{\partial B}{\partial r}=C\,. \tag{1}$$

For the gaseous phase according to Nigmatulin[11] and Luikov[12]

$$A_1=\begin{Bmatrix}\rho_1 r^\alpha\\ \rho_1 V_1 r^\alpha\\ [P/(\gamma-1)+\frac{1}{2}\rho_1 V_1^2]r^\alpha\end{Bmatrix},$$

$$B_1=\begin{Bmatrix}V_1\rho_1 r^\alpha\\ (\rho_1 V_1^2+P)r^\alpha\\ [\gamma P/(\gamma-1)+\frac{1}{2}\rho_1 V_1^2]V_1 r^\alpha\end{Bmatrix}, \tag{2}$$

$$C_1=\begin{Bmatrix}\rho_2 r^\alpha\\ (\alpha r^{\alpha-1}P-\rho_2 M+\delta\rho_2 V_2)r^\alpha\\ (\rho_2\delta Q-\rho_2 V_2 M+\delta\rho_2 V_2^2/2)r^\alpha\end{Bmatrix},$$

and for the solid dispersed phase according to Luikov[12] and Wallis[13]

$$A_2=\begin{Bmatrix}\rho_2 r^\alpha\\ \rho_2 V_2 r^\alpha\\ N r^\alpha\end{Bmatrix},\quad B_2=\begin{Bmatrix}\rho_2 V_2 r^\alpha\\ \rho_2 V_2^2 r^\alpha\\ N V_2 r^\alpha\end{Bmatrix},$$

$$C_2=\begin{Bmatrix}-\delta\rho_2 r^\alpha\\ (\rho_2 M-\delta\rho_2 V_2)r^\alpha\\ 0\end{Bmatrix}, \tag{3}$$

where $\alpha=0$, 1, and 2 denotes planar, cylindrical and spherical symmetry, respectively; ρ is the average density of the component, r is the space variable, V is the velocity, P is the pressure, and M is the drag function related to the exchange of momentum between components [see Eqs. (5)]; γ is the effective isentropic exponent of the gas, N is the number of particles per unit volume, and δ is a variable proportional to the rate of size reduction of the particle [see Eq. (4)]. Variables referring to the gas have the subscript 1, and variables referring to the solid particles have the subscript 2.

Because the energy conservation equation for the solid phase is satisfied trivially (the internal energy is equal to zero), it was replaced with an equation for the conservation of the number of particles. The rate of particle shattering and evaporation δ, is defined by the equation[7]:

$$\delta=K_1\frac{Nu(T_1-T_2)}{\pi l^2\rho_2^i}+K_2(V_1-V_2)^{1/2}l^{-3/2}\,, \tag{4}$$

where T is the temperature, l is the average radius of the particles, and i is the initial value. The coefficients "K_1" (kg/m°Ksec) and "K_2" (m/sec$^{1/2}$) were chosen to fit the experimental values of reaction zone length. The Nusselt number was calculated from the equation

$$\mathrm{Nu}=2+0.6\,\mathrm{Pr}^{0.33}\,\mathrm{Re}^{0.5}\,,$$

where Nu is the Nusselt number, Pr is the Prandtl number, and Re is the Reynolds number. The drag function M was determined according to Borisov *et al.*[14] by

$$M=(3\rho_1/8\rho_2^i)(C_d/l)\,|V_1-V_2|\,(V_1-V_2)\,, \tag{5}$$

where the drag coefficient C_d is dependent on the Reynolds number as follows:

$$C_d=\begin{cases}27\times\mathrm{Re}^{-0.84} & \mathrm{Re}<80\\ 0.27\times\mathrm{Re}^{0.21} & \text{where } 80\leq\mathrm{Re}<10^4\\ 2 & \mathrm{Re}\geq 10^4\,.\end{cases} \tag{6}$$

The initial distribution of gasdynamic parameters behind the shock wave was calculated using the self-similar solution for the deposition of a finite amount of explosive energy as described previously.[15,16] This "starting solution" introduces the initiating charge into the model. Thus, at $t=t_0$ in the region bordered by r_0 the following conditions hold:

$$P=\begin{cases}P(r,t_0), & r\leq r_0\\ P^i, & r>r_0\end{cases};\quad \rho_1=\begin{cases}\rho_1(r,t_0), & r\leq r_0\\ \rho_1^i, & r>r_0\end{cases};$$

$$V=\begin{cases}V_1(r,t_0), & r\leq r_0\\ 0, & r>r_0\end{cases}. \tag{7}$$

The starting parameters for the liquid phase will be

$$l=\begin{cases}0, & r\leq r_0\\ l^i, & r>r_0\end{cases},\quad N=\begin{cases}0, & r\leq r_0\\ N^i, & r>r_0\end{cases}$$

$$V_2=0\,. \tag{8}$$

The system of equations (1)–(3) with boundary conditions (7)–(8) is solved numerically by the flux-corrected transport method described by Boris and Book.[17,18] All cases reported here were calculated with the assumption of spherical symmetry ($\alpha=3$). Details of the numerical solution procedure, code accuracy, and convergence have been described previously.[8]

III. CALCULATIONS OF DYNAMIC AND STATIC IMPULSE

The static impulse of the blast wave of a given point behind the shock front is given by

$$I_s(r,t)=\int_{t_0}^{t}[P(r,t)-P_0]\,dt\,, \tag{9}$$

where $I_s(r,t)$ is the static impulse, P_0 is the initial pressure of the medium, and t_0 is the initial time when

the igniting explosion first reaches the radius r_0.

The dynamic impulse of the wave including the impulse due to both the gas and the particles is given by the expression

$$I_d(r,t) = \int_{t_0}^{t} \frac{1}{2} [\rho_1(r,t)V_1^2(r,t) + \rho_2(r,t)V_2^2(r,t)]dt, \quad (10)$$

where $I_d(r,t)$ is the dynamic impulse.

The integrals (9) and (10) were calculated numerically during the integration of the system (1)–(3). For comparison, the static impulse of a strong point explosion and of a C–J detonation have also been calculated. In these cases the Newton–Cotes formula of the fourth order was used for the approximate integration of Eq. (9). In the case of the point explosion the $P(r,t)$ function was taken from Sedov's analytical solution.[19] In the case of a C–J detonation wave the parameters of the detonation wave in the mixture were determined using the Gordon–McBride program.[20] For simplicity, it was assumed that behind the detonation front the distribution of gasdynamic parameters follows the analytical solution for a planar detonation wave.[21] That will lead to an approximate 10% inaccuracy comparing with the analytical solution for a spherical detonation.

IV. RESULTS AND DISCUSSION

It is obvious that the dynamic and static impulses are mainly dependent on the amount of heat which is liberated in the detonation wave. But the effects of the detonation wave structure and the density of the fuel mixture on the impulse are not clear.

For comparison, the impulse was calculated for a wheat-air mixture and an RDX-air mixture. The parameters of the igniting explosion and the amount of heat release per unit volume were chosen to be the same in both cases. However, since the heat of combustion of RDX is much less than that of wheat, the RDX mass concentration must be more than twice that of wheat, to achieve the same heat release per unit volume of mixture. Figure 1 shows the variation of the pressure and velocity of the gas phase with the radius of the shock wave for an RDX-air mixture.

Each individual curve shows only the first 0.5 m behind the shock so that the agglomeration of lines will not blur the details. Each of the curves corresponds to

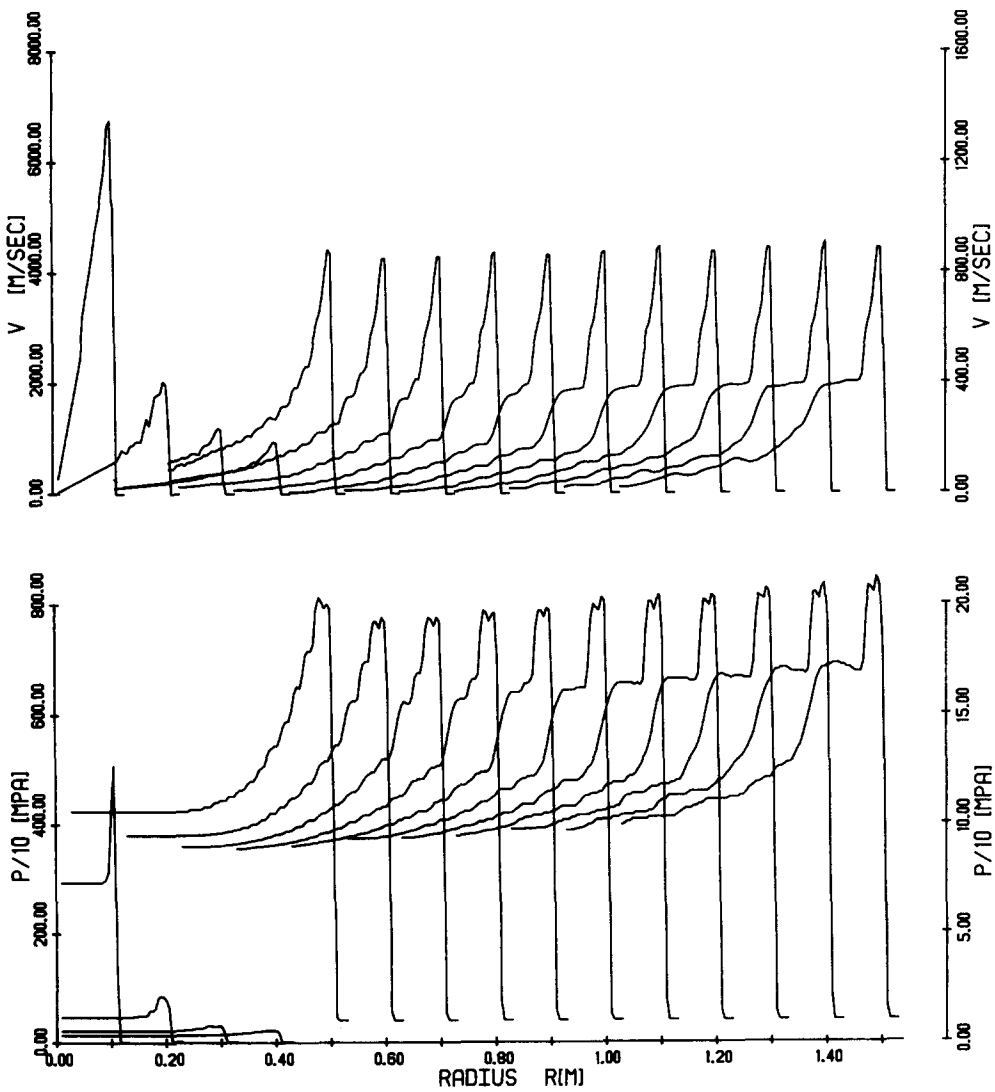

FIG. 1. The pressure and velocity of the gas vs radius for an RDX-air mixture.

TABLE I. Detonation parameters for calculated cases.

	Wheat-air mixture[a]	RDX-air mixture[a]	Decane-oxygen mixture[a]	C–J for Decane-oxygen mixture[b]
E_0(j)	10^6	10^6	10^6	
r_0(m)	0.1	0.1	0.1	
ρ_1^i(kg/m^3)	1.3	1.3	1.3	1.3
P^i(N/m^2)	10^5	10^5	10^5	10^5
T^i(°K)	296	296	296	296
χ(W/m °C)	0.1	0.1	0.1	
l^i(m)$\times 10^4$	0.4	0.4	1	
ρ_2^i(kg/m^3)	1450	1600	730	
Q(j/kg)$\times 10^{-6}$	15.3	6.72	40	40
F/A	0.4122	0.94	0.1577	0.1577
D(m/sec)	1380	1200	1600	2045
P_{RZ}(N/m^2)$\times 10^{-5}$	14.7	15	16	28.3
P_{sh}(N/m^2)$\times 10^{-5}$	24	20	30	
ρ_{RZ}/ρ_1^i	1.4	2.	1.25	1.85
ρ_{sh}/ρ_1^i	4.0	3.8	4.5	
RZ(cm)	12.5	13	10	

[a]Numerical analysis[20].
[b]Gordon–McBride.

a specific shock radius. The velocity and pressure curves for the same instant of time are below one another. The function scale for the first four radii are shown on the left-hand side, while the scale for the other radii is on the right. The parameters of the igniting explosion were taken to be the same in all calculations and are: $E_0 = 10^6$ J; $r_0 = 0.1$ m. The parameters of both phases and the fuel-air ratio for the RDX-air mixture are presented in Table I.

Figure 2 shows the variation of pressure and velocity of the gas phase with the radius of the shock wave for the wheat-air mixture. The parameters of the igniting explosion are the same as in the previous case. The parameters used for the wheat-air mixture are presented in Table I.

The amount of heat liberated in units of mixture volume in these two cases is the same: 8.2×10^6 J/m^3. The reaction zone length is 13 cm for both cases and the dynamics of heat release behind the shock wave is also the same.

Figures 1 and 2 show the difference in the structure of the detonation waves in these two mixtures. The peak velocity and pressure are higher in the case of the wheat-air detonation, but then decrease faster behind the shock wave than in the case of RDX. Because of the higher concentration of particles in the RDX-air mixture, the pressure plateau immediately behind the shock wave is wider in this case.

Comparing the peak pressure for the RDX-air and wheat-air mixtures in Table I it is found that the wheat-air mixture has a 20% higher shock pressure, but at the same time the pressures P_{CJ} at the end of the reaction zone are approximately 15×10^5 N/m^2 in both cases.

In Fig. 3 the values of the static impulse behind the shock front are shown for the two cases when the shock has a radius of 1.5 m. This figure shows how the difference in the density of the mixture and in the structure of the detonation wave can influence the impulse. The static impulse of the RDX-air mixture is higher because the region of high pressure is wider and the shock wave velocity is lower in this case. At the same time the RDX-air detonation produces a lower dynamic impulse (as can be seen in Fig. 4), because the velocity induced by the detonation is much lower than in the case of the wheat-air detonation as is evident from Figs. 1 and 2. The decrease in the dynamic impulse values after reaching a maximum at the end of the reaction zone, can be explained by the nature of the detonation wave development. It is evident from Figs. 1 and 2 that the detonation velocity has a minimum value at the radius of about 0.6 m, and from this point begins to accelerate. The dynamics of the detonation wave development depend mainly on the length of the reaction zone,[22] and the location of the point where the detonation velocity reaches a minimum depends on the igniting explosion parameters.[7]

Figure 5 shows values of the dynamic and static impulse up to a distance of approximately 20 cm behind the shock wave for the wheat-air and RDX-air detonations. From this plot it is possible to see that for a short distance behind the shock wave front ($\simeq$ 5 cm), the values of the dynamic and static impulse are of the

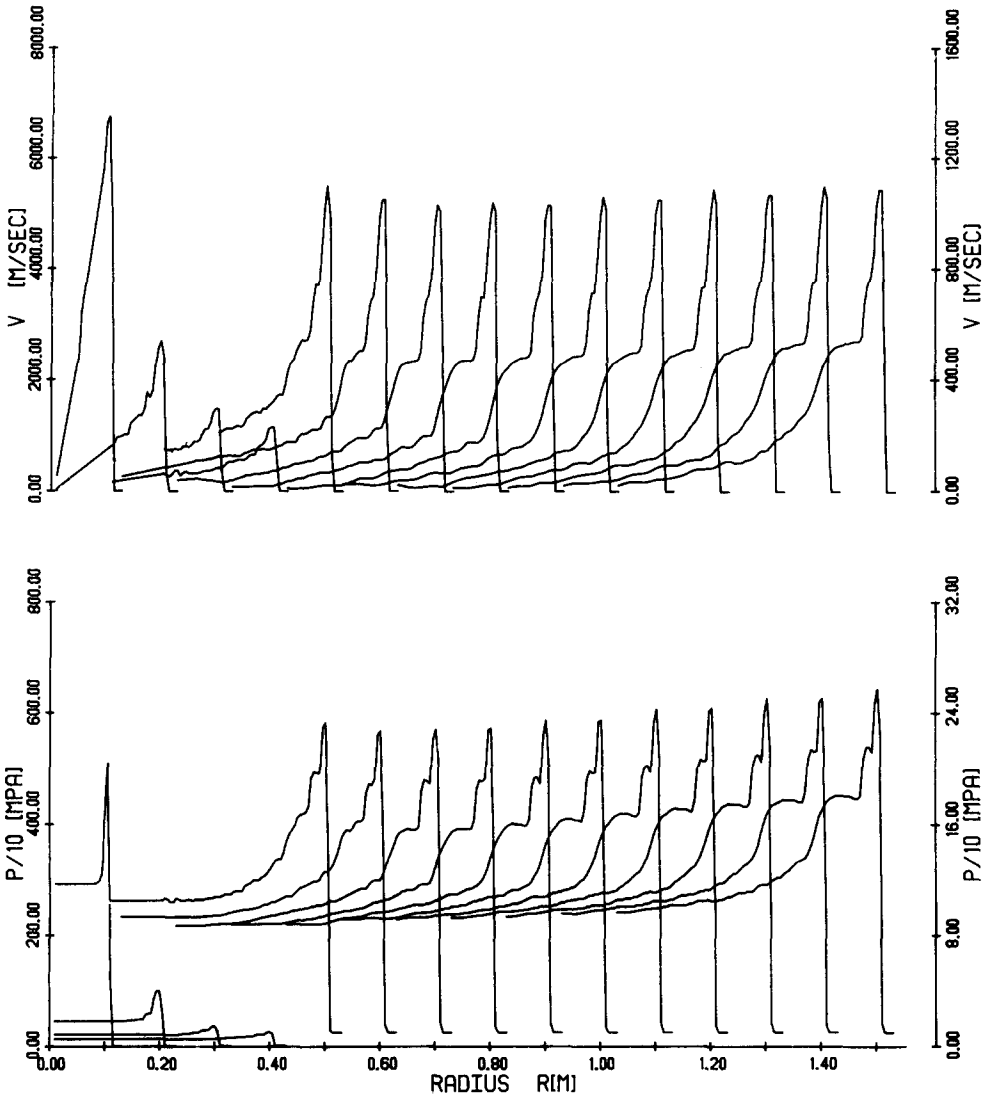

FIG. 2. The pressure and velocity of the gas vs radius for a wheat-air mixture.

same order of magnitude; however, farther behind the shock the static impulse becomes much higher than the dynamic impulse. This behavior can be explained by the rapid drop in the mass velocity behind the shock front. The dynamic impulse of the particles was also determined and was found to be from only 2% up to 5% of the total dynamic impulse.

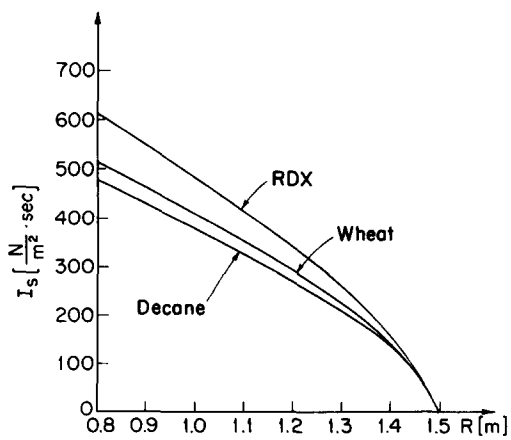

FIG. 3. Static impulse vs radius for different two-phase mixtures.

Figures 3 and 4 also show the static and dynamic impulse for a mixture of decane droplets and oxygen since it is of interest to compare the behavior of spray and dust detonations. The mixture parameters for this case are also shown in Table I. The mass of fuel in the mixture was approximately 40% of the mass of wheat in the wheat-air mixture, because decane has a higher value of heat of combustion per unit mass of fuel and its concentration was chosen to give the same value of heat release per unit volume as in wheat-air and RDX-air detonations. Comparing the decane-oxygen detonation dynamic and static impulses with the two previous calculations, it can be seen that there is an additional increase in the dynamic impulse and a decrease in the static impulse.

In the present analysis the exchange of heat between the gas and the particles is neglected. In the real case the differences between the values of the static and dynamic impulse could be even greater because with the increase in particle concentration the effective ratio of specific heats of the mixture decreases because of

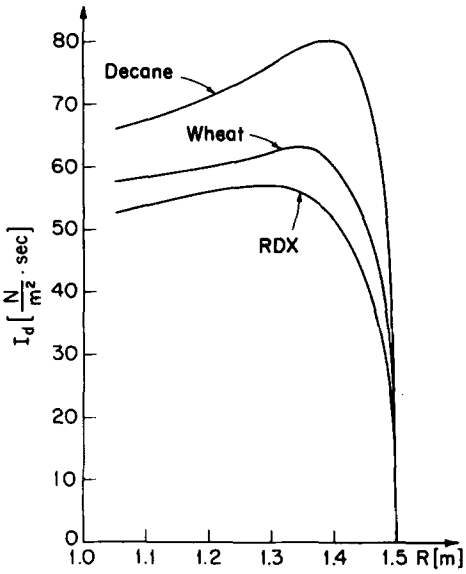

FIG. 4. Dynamic impulse vs radius for different combustible mixtures.

gas-particle heat exchange. This effect would lead to an additional decrease in the pressure and velocity behind the shock wave.

The reaction zone lengths in all cases presented in Figs. 3 and 4 are approximately equal, and it has been shown that different impulse values are obtained because the different mass concentrations of solid or liquid phase modify the detonation wave structure.

To find out how the reaction zone length influences the impulse two examples were calculated in which the only difference was the radius of the particles. Consequently the different particle burning rates behind the shock front result in different reaction zone lengths.

In Fig. 6 the dynamic impulses are shown for mixtures of RDX and air. One mixture was taken with the parameters given in Table I and in the second mixture only the particle radius l' was increased from 40–60 μm.

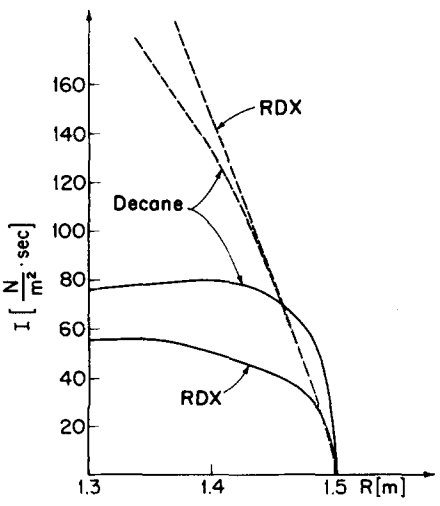

FIG. 5. Calculated dynamic (solid lines) and static (dashed lines) impulses vs radius in the vicinity of the shock front.

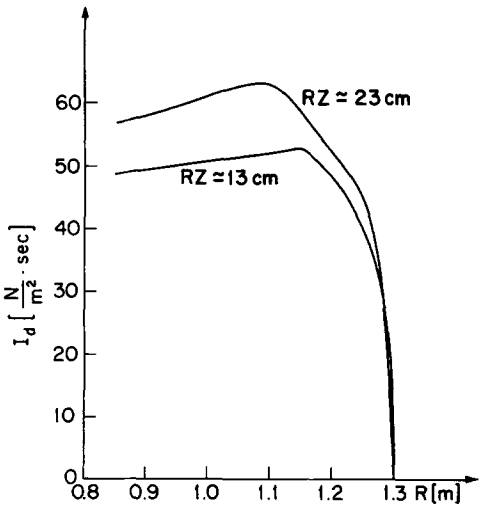

FIG. 6. Calculated dynamic impulse vs radius for cases with different reaction zone length.

The corresponding reaction zone lengths are 13 and 23 cm, respectively. The detonation parameters for the 40 and 60 μm particles were: $P_{sh}=20$ atm, $P_{RZ}=15$ atm, $D=1200$ m/sec, and $P_{sh}=16$ atm, $P_{RZ}=11.5$ atm, $D=1100$ m/sec, respectively.

It can be seen that the dynamic impulse reaches its maximum value at the end of the reaction zone in both cases after which it decreases. In the region very close to the front of the shock wave the value of the dynamic impulse for the case with the shorter reaction zone (RZ) is higher but the detonation wave with the larger reaction zone finally has a higher dynamic impulse because of the wider region with a high mass velocity.

The calculations show that the case with the shorter reaction zone gives static impulses about 10% larger. However, beyond a distance of about 23 cm the values of static impulse became equal for both cases. The difference in the region closer to the shock front can be explained by the higher pressure in this region in the case of the shorter reaction zone.

Figure 7 shows the dynamics of change of the static impulse in the process of the detonation wave development. It can be seen that the static impulse graphs for the developed detonation wave for decane and RDX are represented by approximately parallel curves (compare the broken and solid lines at wave radii of 1 and 1.5 m). For the shorter radii when the propagation of the shock wave is still influenced by the igniting explosion, the shapes of the graphs are different. The density of the mixture significantly changed the static impulse value from the first moments of the blast propagation into the two-phase medium, and this effect increases with increasing wave radius.

Figure 7 also shows the impulse obtained using the analytical solution for a strong point explosion and the impulse from a Chapman–Jouguet detonation with zero-reaction zone length. The energy of explosion for the

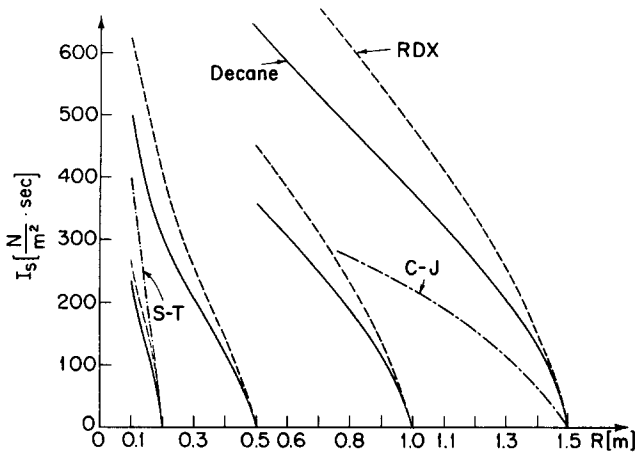

FIG. 7. Calculated static impulse vs radius for decane-oxygen detonation (solid lines) for RDX-air detonation (dashed line), for point explosion (S–T) and Chapman–Jouguet detonation (C–J).

point explosion was equal to the energy of the igniting explosion in the two-phase calculation.

The dot-dash line starting at the 0.2 m radius indicates that the impulse value which follows from the assumption that the shock wave was the result of a strong point explosion without counterpressure. The results obtained are in agreement with Fishburn's[3] calculations which also indicated higher values of the static impulse calculated with the assumption of a strong point explosion.

The dot-dash line coming from the 1.5 m radius shows the impulse value calculated using the assumption that the wave is an ideal gaseous C–J detonation wave. The C–J conditions for the decane-oxygen mixture were calculated using the Gordon–McBride[20] computer code and are included in Table I. The calculated value of the C–J detonation static impulse is smaller than that of the corresponding two-phase decane oxygen detonation and supports the conclusions about the influence of the reaction zone and density on the impulse value.

V. CONCLUSIONS

In this study using numerical simulation of the direct initiation and propagation of detonation waves in two-phase media it was found that:

(a) Increasing the mass concentrations of the solid or liquid phase led to an increase in the static impulse and a decrease in the dynamic impulse.

(b) Decreasing the reaction zone length resulted in a slight increase in the static impulse and a decrease in the dynamic impulse.

(c) The dynamic impulse reached its maximum value at the end of the reaction zone behind the front of the shock wave. This effect is related to the detonation wave acceleration in the region considered in the calculations.

(d) The difference in the static impulse value is due mainly to longer exposure to high pressure in cases when the shock wave moved more slowly in the medium due to a higher concentration of the condensed phase.

(e) The difference in the value of the dynamic impulse value is due mainly to the difference in the structure of the wave.

[1]H. L. Brode, RAND Corporation Report RM-1825-AEC, Santa Monica, California (1956).
[2]H. L. Brode, Phys. Fluids 2, 217 (1959).
[3]B. D. Fishburn, Acta Astronaut. 3, 1043 (1976).
[4]N. M. Sternberg and N. Hurwitz, *Sixth Symposium on Detonation* (Office of Naval Research, Washington, D.C., 1976), p. 528.
[5]J. A. Nicholls, *Fast Reactions in Energetic Systems* (NATO Advanced Study Institute, Greece, 1980).
[6]C. W. Kauffman, P. Wolanski, E. Ural, J. A. Nicholls, and R. VanDyk, in *Proceedings of the International Symposium on Grain Dust*, edited by B. S. Miller and Y. Pomeranz (Division of Continuing Education, Kansas State University, Manhattan, Kansas, 1979), p. 164.
[7]S. Eidelman and A. Burcat, AIAA J. 18, 1103 (1980).
[8]S. Eidelman and A. Burcat, J. Comput. Phys. **39**, 456 (1981).
[9]E. A. Antonov and A. M. Gladilin, Isv. Akad. Nauk. Mekh. Zhidk Gaza, No. 5, 92 (1972).
[10]H. Krier and A. Mozaffarian, Int. J. of Multiphase Flow 4, 65 (1978).
[11]R. N. Nigmatulin, *Fundamentals of the Mechanics of Heterogenous Media* (Nauka, Moskva, 1978).
[12]A. V. Luikov, *Heat Mass Transfer* (Izd. Energia, Moskva, 1972).
[13]G. B. Wallis, *One-Dimensional Two-Phase Flow* (McGraw-Hill, New York, 1970).
[14]A. A. Borisov, B. E. Gelfand, S. A. Gubin, S. M. Kogarko, and A. L. Podgrebenkov, Combust. Exp. Shock Waves 6, 372 (1970).
[15]S. Eidelman, Y. M. Timnat, and A. Burcat, in *6th Symposium on Detonation* (Office of Naval Research, Washington, D.C., 1976), p. 590.
[16]A. Burcat, S. Eidelman, and Y. Manheimer-Timnat, *Symposium on High Dynamic Pressures* (Commisariat a le Energie Atomique, Paris, 1978), p. 347.
[17]J. P. Boris and D. L. Book, J. Comput. Phys. 11, 38 (1973).
[18]J. P. Boris and D. L. Book, in *Methods in Computational Physics*, (Academic, New York, 1976), Vol. 16, Chap. III.
[19]L. I. Sedov, *Similarity and Dimensional Methods in Mechanics* (Infosearch, London, 1959).
[20]S. Gordon and B. J. McBride, NASA SP-273 (1971).
[21]F. A. Baum, L. P. Orlenko, K. P. Stanyukovich, V. P. Chelishev, and B. I. Shekhter, *The Physics of Explosion*, edited by K. P. Stanyukovich (Nauka, Moskva, 1975).
[22]R. Bar-Or, M. Sichel, and J. A. Nicholls, in *18th Combustion Symposium*. (The Combustion Institute, Pittsburg, Pennsylvania, 1981), p. 1599.